

D MESON ENHANCEMENT IN *pp* COLLISIONS AT THE LHC DUE TO NONLINEAR GLUON EVOLUTION

A. Dainese¹,

University of Padova and INFN, via Marzolo 8, 35131 Padova, Italy

R. Vogt²,

*Lawrence Berkeley National Laboratory, Berkeley, CA 94720, USA
Physics Department, University of California, Davis, CA 95616, USA*

M. Bondila³, K.J. Eskola⁴, and V.J. Kolhinen⁵

*Department of Physics, P.O. Box 35, FIN-40014 University of Jyväskylä, Finland
Helsinki Institute of Physics, P.O. Box 64, FIN-00014 University of Helsinki, Finland*

Abstract

When nonlinear effects on the gluon evolution are included with constraints from HERA, the gluon distribution in the free proton is enhanced at low momentum fractions, $x \lesssim 0.01$, and low scales, $Q^2 \lesssim 10 \text{ GeV}^2$, relative to standard, DGLAP-evolved, gluon distributions. Consequently, such gluon distributions can enhance charm production in *pp* collisions at center of mass energy 14 TeV by up to a factor of five at midrapidity, $y \sim 0$, and transverse momentum $p_T \rightarrow 0$ in the most optimistic case. We show that most of this enhancement survives hadronization into *D* mesons. Assuming the same enhancement at leading and next-to-leading order, we show that the *D* enhancement may be measured by D^0 reconstruction in the $K^-\pi^+$ decay channel with the ALICE detector.

¹andrea.dainese@pd.infn.it

²vogt@lbl.gov

³mariana.bondila@phys.jyu.fi

⁴kari.eskola@phys.jyu.fi

⁵vesa.kolhinen@phys.jyu.fi

1 Introduction

The parton distribution functions, PDFs, of the free proton are determined through global fits obtained using the leading-order, LO, next-to-leading order, NLO, or even next-to-next-to-leading order, NNLO, formulation of the Dokshitzer, Gribov, Lipatov, Altarelli and Parisi, DGLAP, scale evolution equations [1]. In particular, the HERA data on the proton structure function $F_2(x, Q^2)$ [2] as a function of Bjorken- x and squared momentum transfer Q^2 , and, especially, the Q^2 slope, $\partial F_2(x, Q^2)/\partial \ln Q^2$, in the small- x , $3 \times 10^{-5} \lesssim x \lesssim 5 \times 10^{-3}$, and small- Q^2 region, $1.5 \lesssim Q^2 \lesssim 10 \text{ GeV}^2$, set rather stringent constraints on the small- x gluon distributions. The agreement of the global fits with the measured $F_2(x, Q^2)$ is, in general, very good but certain problems arise. When the small- x and small- Q^2 region is included in the DGLAP fits, they are not as good as the excellent ones obtained at larger values of x and Q^2 [3]. In addition, some NLO gluon distributions [4] become negative at small x for Q^2 on the order of a few GeV^2 .

The kernels of the DGLAP equations only describe splitting of one parton into two or more so that the resulting equations are linear in the PDFs. This ignores the fact that, at low Q^2 , the small- x gluon density may increase to the point where gluon fusion becomes significant. These fusions generate nonlinearities in the evolution equations. The first nonlinear corrections, the GLRMQ terms, were derived by Gribov, Levin and Ryskin and also by Mueller and Qiu [5]. Eventually, at even smaller x and Q^2 , nonlinearities are expected to dominate the evolution to all orders. This fully nonlinear region, where both the linear DGLAP evolution and the GLRMQ-corrected DGLAP evolution are inapplicable, is the gluon saturation region, see e.g. Ref. [6].

Outside the saturation region, incorporating the nonlinearities may improve the global fits when the small- x and Q^2 regions are included. Recent work in Ref. [7], where the LO DGLAP evolution equations were supplemented by the GLRMQ terms, showed that the nonlinearly-evolved PDFs reproduce the HERA F_2 measurements at $x \gtrsim 3 \times 10^{-5}$ and $Q^2 \gtrsim 1.5 \text{ GeV}^2$ [2] equally well or even better than the conventional LO PDFs such as CTEQ6L [8]. The nonlinearly-evolved gluon distributions at $Q^2 \lesssim 10 \text{ GeV}^2$ and $x \lesssim 0.01$, however, were clearly enhanced relative to CTEQ6L and CTEQ61L [9]. As shown in Fig. 1 of Ref. [10], the enhancement arises because the nonlinear evolution is slower than DGLAP alone. At higher x and Q^2 the nonlinear and linear evolution of the gluon distributions should become very similar to fit the same data. An enhancement can also be expected at NLO. However, since the NLO small- x gluon distributions are typically reduced relative to LO, at NLO the enhancement may be smaller than at LO [3].

Since the same HERA data can be reproduced by linear evolution starting from a relatively flat gluon distribution and by nonlinear evolution with clearly enhanced small- x gluons, other observables are necessary to probe the effects of the nonlinearities. In Ref. [10], charm production in pp collisions at the LHC was suggested as a promising candidate process. Due to gluon dominance of charm production and the small values of x and Q^2 probed, $x \approx 2 \times 10^{-4}$ and $Q^2 \approx 1.69 - 6 \text{ GeV}^2$ at midrapidity and

transverse momentum¹ $p_T \approx 0$, charm production at the LHC is sensitive to the gluon enhancement. The resulting charm enhancement was quantified in Ref. [10] by the LO ratios of the differential cross sections computed with the nonlinearly-evolved EHKQS PDFs [7], obtained from DGLAP+GLRMQ evolution, relative to the DGLAP-evolved CTEQ61L PDFs.

The enhancement of the nonlinearly-evolved gluons increases as x and Q^2 decrease. Consequently, the charm enhancement increases with center of mass energy, \sqrt{s} . Thus the maximum enhancement at the LHC will be at $\sqrt{s} = 14$ TeV and small charm quark transverse momentum. The sensitivity of the charm enhancement to the value of the charm quark mass, m_c , as well as to the choice of the factorization, Q_F^2 , and renormalization, Q_R^2 , scales was studied in Ref. [10] assuming $Q^2 = Q_F^2 = Q_R^2 \propto m_T^2$, the charm transverse mass squared, $m_T^2 = p_T^2 + m_c^2$. For the most significant charm enhancement, m_c and Q^2/m_T^2 should both be small. A comparison of the NLO total cross sections with low energy data shows that the data prefer such small m_c and Q^2 combinations [11, 12]. The smallest scales and thus the largest enhancement are obtained with $m_c = 1.3$ GeV and $Q^2 = m_T^2$. In this case, the ratio of the inclusive differential cross section, $d^3\sigma/dp_T dy_1 dy_2$, computed with EHKQS set 1 relative to CTEQ61L is greater than 5 for rapidities $|y, y_2| \lesssim 2$ where y and y_2 are the c and \bar{c} rapidities, respectively.

In Ref. [10], the enhancement was described only for charm production. Neither its subsequent hadronization to D mesons nor its decay and detection were considered. In this paper, we address these issues to determine whether the charm enhancement survives hadronization and D decay. At the LHC, the ALICE detector [13] is perhaps in the best position for measuring such an enhancement since it is capable of reconstructing D^0 hadronic decays down to very low transverse momentum.

We first consider how much of the LO charm enhancement survives in the final state D meson distributions. Charm quarks are hadronized using the PYTHIA string fragmentation model [14]. We show that, for the most optimistic case with a factor of five charm enhancement for $p_T \rightarrow 0$, the D enhancement is a factor of three for $p_T^D \rightarrow 0$.

Since the ALICE detector allows direct measurement of the D meson p_T distribution through D^0 reconstruction in the $K^-\pi^+$ decay channel, we then determine whether or not the surviving D enhancement can be detected above the expected experimental statistical and systematic uncertainties. To determine realistic statistical uncertainties, we calculate the NLO cross section in the way most compatible with our LO enhancement, as described below. Then, using the error analysis developed by one of us (A.D.) in Ref. [15], we demonstrate that detection of the enhancement is possible.

Finally, we consider whether NLO charm cross sections, calculated with linearly-evolved PDFs and different combinations of m_c , Q_F^2 and Q_R^2 , can mimic the charm enhancement. Our results show that this is unlikely.

This paper is organized as follows. In Section 2, we describe our charm calculations and define how the NLO cross section most compatible with the LO enhancement is

¹Here we use p_T for the transverse momentum of the charm quark and p_T^D for the transverse momentum of the D meson.

computed. Hadronization and reconstruction of D^0 mesons are considered in Sections 3 and 4, respectively, along with a discussion of the experimental uncertainties. We then generate “data” based on the enhanced cross sections and the experimental uncertainties. These data are then compared to compatible NLO calculations to learn whether the enhancement is measurable for a unique set of parameters in Section 5. We conclude in Section 6.

2 Charm enhancement from nonlinear PDF evolution

According to collinear factorization, the inclusive differential charm hadroproduction cross sections at high energies can be written as

$$d\sigma_{pp \rightarrow c\bar{c}X}(\sqrt{s}, m_c, Q_R^2, Q_F^2) = \sum_{i,j=q,\bar{q},g} f_i(x_1, Q_F^2) \otimes f_j(x_2, Q_F^2) \otimes d\hat{\sigma}_{ij \rightarrow c\bar{c}\{k\}}(\alpha_s(Q_R^2), Q_F^2, m_c, x_1, x_2), \quad (1)$$

where $d\hat{\sigma}_{ij \rightarrow c\bar{c}\{k\}}$ is the perturbative partonic hard part, calculable as a power series in the strong coupling $\alpha_s(Q_R^2)$. The proton PDFs for each parton $i(j)$ at fractional momentum $x_1(x_2)$ and factorization scale Q_F^2 are denoted by $f_i(x, Q_F^2)$. At LO, where $d\hat{\sigma} \propto \alpha_s^2(Q_R^2)$, only the subprocesses $gg \rightarrow c\bar{c}$ and $q\bar{q} \rightarrow c\bar{c}$ are allowed [16] so that $\{k\} = 0$. At NLO, where $d\hat{\sigma} \propto \alpha_s^3(Q_R^2)$, subprocesses where $\{k\} \neq 0$, e.g. $gg \rightarrow c\bar{c}g$ and $gq \rightarrow c\bar{c}q$ contribute. The gq channel, new at NLO, only contributes a few percent of the total cross section.

The charm production enhancement studied here and in Ref. [10] results from the nonlinearly-evolved EHKQS PDFs² where the gluon distribution is enhanced for $x \lesssim 0.01$ at the few-GeV scales. The EHKQS PDFs were constructed in Ref. [7] using CTEQ5L [17] and CTEQ6L as baselines with the HERA data [2] as constraints. The EHKQS sets have initial scale $Q_0^2 = 1.4 \text{ GeV}^2$ and a four-flavor Λ_{QCD} value of $\Lambda_{\text{QCD}}^{(4)} = 0.192 \text{ GeV}$. Following Ref. [10], we quantify the charm enhancement against charm production computed with the CTEQ61L LO PDFs where the data were fit with the one-loop α_s . The CTEQ61L set takes $Q_0^2 = 1.69 \text{ GeV}^2$ and $\Lambda_{\text{QCD}}^{(4)} = 0.215 \text{ GeV}$. For consistency, we calculate α_s at one loop with the appropriate value of $\Lambda_{\text{QCD}}^{(4)}$ for each set.

Previously [10], we worked at LO only since the EHKQS sets are evolved according to the LO DGLAP+GLRMQ equations using a one-loop evaluation of α_s . Thus these LO distributions should generally not be mixed with NLO matrix elements and the two-loop α_s . However, the charm quark total cross section is increased and the p_T distribution is broadened at NLO relative to LO [18]. Thus, to determine whether or not the enhancement is experimentally measurable, we must go beyond the ratio presented in Ref. [10]. To accomplish this, we assume that the enhancement will be the same at NLO as at LO and employ a NLO cross section closest to the calculation of the enhancement in Ref. [10].

²These PDFs are available at www.urhic.phys.jyu.fi.

As described in Ref. [18], the theoretical K factor may be defined in more than one way, depending on how the LO contribution to the cross section is calculated. In all cases, the $\mathcal{O}(\alpha_s^3)$ contribution to cross section is calculated using NLO PDFs and the two-loop evaluation of α_s . If the LO contribution is also calculated using NLO PDFs and a two-loop α_s , this is the “standard NLO” cross section. It is used in most NLO codes, both in the global analyses of the NLO PDFs and in evaluations of cross sections and rates [18]. The K factor formed when taking the ratio of the “standard NLO” cross section to the LO cross section with the NLO PDFs [18], $K_0^{(1)}$, indicates the convergence of terms in a fixed-order calculation [19]. On the other hand, if the LO contribution to the total NLO cross section employs LO PDFs and the one-loop α_s , we have a cross section which we refer to here as “alternative NLO”. The K factor calculated taking the ratio of the “alternative NLO” cross section to the LO cross section with LO PDFs [18], $K_2^{(1)}$, indicates the convergence of the hadronic cross section toward a result. If $K_0^{(1)} > K_2^{(1)}$, convergence of the hadronic cross section is more likely [19]. This is indeed the case for charm production [18]. We also note that $K_2^{(1)}$ is a much weaker function of energy than $K_0^{(1)}$. Since, in the absence of nonlinear NLO PDFs, the “alternative NLO” cross section is more consistent with the enhancement calculated in Ref. [10], we use this cross section to calculate the NLO D meson rates and p_T spectra. We note also that, in both cases, the p_T distributions have the same slope even though $K_2^{(1)}$, for the alternative NLO cross section, is somewhat smaller. Thus, using a non-standard NLO calculation will not change the slope of the p_T distributions, distorting the result.

The LO and NLO calculations used to obtain the full NLO result in both cases can be defined by modification of Eq. (1). For simplicity, we drop the dependence of the cross section on \sqrt{s} , m_c , Q_F^2 and Q_R^2 on the left-hand side of Eq. (1) in the following. We thus define the full LO charm production cross section as

$$d\sigma_{\text{LO}}^{\text{1L}} = \sum_{i,j=q,\bar{q},g} f_i^{\text{LO}}(x_1, Q_F^2) \otimes f_j^{\text{LO}}(x_2, Q_F^2) \otimes d\hat{\sigma}_{ij \rightarrow c\bar{c}}^{\text{LO}}(\alpha_s^{\text{1L}}(Q_R^2), x_1, x_2) \quad (2)$$

where the superscript “LO” on $d\hat{\sigma}_{ij \rightarrow c\bar{c}}$ indicates the use of the LO matrix elements while the superscript “1L” indicates that the one-loop expression of α_s is used. The LO cross section typically used in NLO codes employs the NLO PDFs and the two-loop (2L) α_s so that

$$d\sigma_{\text{LO}}^{\text{2L}} = \sum_{i,j=q,\bar{q},g} f_i^{\text{NLO}}(x_1, Q_F^2) \otimes f_j^{\text{NLO}}(x_2, Q_F^2) \otimes d\hat{\sigma}_{ij \rightarrow c\bar{c}}^{\text{LO}}(\alpha_s^{\text{2L}}(Q_R^2), x_1, x_2) . \quad (3)$$

In either case, the NLO contribution, $\mathcal{O}(\alpha_s^3)$ for heavy quark production, is

$$d\sigma_{\mathcal{O}(\alpha_s^3)} = \sum_{i,j=q,\bar{q},g} f_i^{\text{NLO}}(x_1, Q_F^2) \otimes f_j^{\text{NLO}}(x_2, Q_F^2) \otimes \sum_{k=0,q,\bar{q},g} d\hat{\sigma}_{ij \rightarrow c\bar{c}k}^{\text{NLO}}(\alpha_s^{\text{2L}}(Q_R^2), Q_F^2, x_1, x_2) \quad (4)$$

where the superscript “NLO” on $d\hat{\sigma}_{ij \rightarrow c\bar{c}k}$ indicates the use of the NLO matrix elements. The additional sum over k in Eq. (4) includes the virtual, $k = 0$, and real, $k = q, \bar{q}$ or g depending on i and j , NLO corrections. In the calculations of $d\sigma_{\text{LO}}^{\text{2L}}$ and $d\sigma_{\mathcal{O}(\alpha_s^3)}$,

we use the value of $\Lambda_{\text{QCD}}^{(4)}$ given for the NLO PDFs and work in the $\overline{\text{MS}}$ scheme. The standard NLO cross section is then

$$d\sigma_{\text{NLO}}^{\text{std}} = d\sigma_{\text{LO}}^{2\text{L}} + d\sigma_{\mathcal{O}(\alpha_s^3)} \quad (5)$$

while our ‘‘alternative NLO’’ cross section is defined as

$$d\sigma_{\text{NLO}}^{\text{alt}} = d\sigma_{\text{LO}}^{1\text{L}} + d\sigma_{\mathcal{O}(\alpha_s^3)} . \quad (6)$$

Since the enhancement in Ref. [10] was defined using $d\sigma_{\text{LO}}^{1\text{L}}$ only, the best we can do is to use the alternative NLO cross section in our analysis, as described below.

We now discuss how the enhancement is taken into account in the context of the NLO computation. We calculate the LO inclusive charm p_T distribution, $d^2\sigma/dp_T dy$, with the detected charm (anticharm) quark in the rapidity interval Δy with $|y| < 1$, motivated by the pseudorapidity acceptance of the ALICE tracking barrel, $|\eta| < 0.9$. The rapidity, y_2 , of the undetected anticharm (charm) quark is integrated over. The charm enhancement factor $R(p_T, \Delta y)$ is then

$$R(p_T, \Delta y) = \frac{\int_{\Delta y} dy \int dy_2 \frac{d^3\sigma(\text{EHKQS})}{dp_T dy dy_2}}{\int_{\Delta y} dy \int dy_2 \frac{d^3\sigma(\text{CTEQ61L})}{dp_T dy dy_2}} . \quad (7)$$

Numerically, this ratio is very close to $R(p_T, y, y_2)$, computed in Ref. [10], as seen by a comparison of $R(p_T, \Delta y)$ in Fig. 1 with Fig. 2 of Ref. [10].

Next, we assume that the enhancement calculated at LO is the same when calculated at NLO. This is a rather strong assumption but, until the nonlinear evolution has been completely analyzed to NLO, it is the only reasonable assumption we can make to test whether the enhancement can be detected with ALICE which will measure the physical p_T^2 distribution. The alternative NLO cross section is therefore the closest in spirit to the LO computation in Ref. [10]. Thus, the enhanced NLO charm p_T distribution is

$$R(p_T, \Delta y) d\sigma_{\text{NLO}}^{\text{alt}}(\Delta y)/dp_T . \quad (8)$$

In our calculations, we use values of the charm quark mass and scale that have been fit to the total cross section data using standard NLO calculations. The best agreement with the total cross section data is obtained with $m_c = 1.2$ GeV and $Q^2 = 4m_c^2$ for DGLAP-evolved NLO PDFs such as CTEQ6M [9] and MRST [20]. Nearly equivalent agreement may be obtained with $m_c = 1.3$ GeV and $Q^2 = m_c^2$ [11, 12]. Agreement with the fixed-target total cross sections can only be achieved with higher m_c by making the factorization scale, Q_F^2 , larger than the renormalization scale, Q_R^2 . Using a lower value of Q_R^2 increases the cross section by inflating α_s . If $Q_F^2 \leq Q_R^2$, the PDFs are unconstrained in Q^2 and are thus unreliable. We keep $Q_F^2 = Q_R^2$ since all typical PDFs are fit using this assumption. Thus we limit ourselves to relatively small values of m_c to obtain agreement with the total cross section data.

We note that while m_c is the only relevant scale in the total cross section, m_T is used instead of m_c in the calculations of R and $d\sigma_{\text{NLO}}^{\text{alt}}(\Delta y)/dp_T$ to control p_T -dependent logarithms at NLO [10]. Our main results are then based on the inputs that give the best agreement with the total cross section data, $m_c = 1.2$ GeV and $Q^2 = 4m_T^2$ as well as $m_c = 1.3$ GeV and $Q^2 = m_T^2$. These two choices will form the baseline results against which other parameter choices will be compared to see if the enhancement can be detected.

3 From charm to D enhancement

Previously [10], we did not include parton intrinsic transverse momentum, k_T , broadening or fragmentation. Since the effect of intrinsic k_T is quite small at LHC energies, on the order of 10% or less [11], we have not included intrinsic k_T in our calculations. To make a more realistic D meson distribution, we have modified the charm p_T distribution by the heavy quark string fragmentation in PYTHIA [14], as explained below. The resulting D distribution is significantly harder than that obtained using the Peterson fragmentation function [21].

We first show how the p_T -dependent enhancement, calculated for the charm quark, is reflected in the D meson p_T distribution. Charm events in pp collisions at $\sqrt{s} = 14$ TeV are generated using PYTHIA (default settings) with the requirement that one of the quarks is in the interval $|y| < 1$. The charm quarks are hadronized using the default string model. Since c and \bar{c} quarks fragment to D and \bar{D} mesons³, respectively, in each event related (c, D) and (\bar{c}, \bar{D}) pairs can easily be identified⁴. These pairs are reweighted to match an arbitrary NLO charm quark p_T distribution, dN_{NLO}^c/dp_T . If $dN_{\text{PYTHIA}}^c/dp_T$ is the charm p_T distribution given by PYTHIA, each (c, D) pair is assigned the weight

$$\mathcal{W}(p_T) = \frac{dN_{\text{NLO}}^c/dp_T}{dN_{\text{PYTHIA}}^c/dp_T} \quad (9)$$

where p_T is the transverse momentum of the charm quark of the pair. Therefore, the reweighted final-state D distribution corresponds to the one that would be obtained by applying string fragmentation to the NLO c -quark distribution.

In Fig. 1 we compare the enhancement factor R , calculated in Eq. (7) for c quarks and D mesons generated from the weighted PYTHIA charm distributions. The two cases described previously, $m_c = 1.2$ GeV, $Q^2 = 4m_T^2$ (left-hand side) and $m_c = 1.3$ GeV, $Q^2 = m_T^2$ (right-hand side) are considered. In both cases, the enhancement survives after fragmentation. It is interesting to note that the D enhancement is somewhat lower than that of the charm: in the most optimistic case, the factor of five charm enhancement has reduced to a factor of three for the D mesons. This occurs because, for a given p_T^D , the D spectrum receives contributions from charm quarks with

³Here $D \equiv D^+, D^0$.

⁴Events containing charm baryons were rejected.

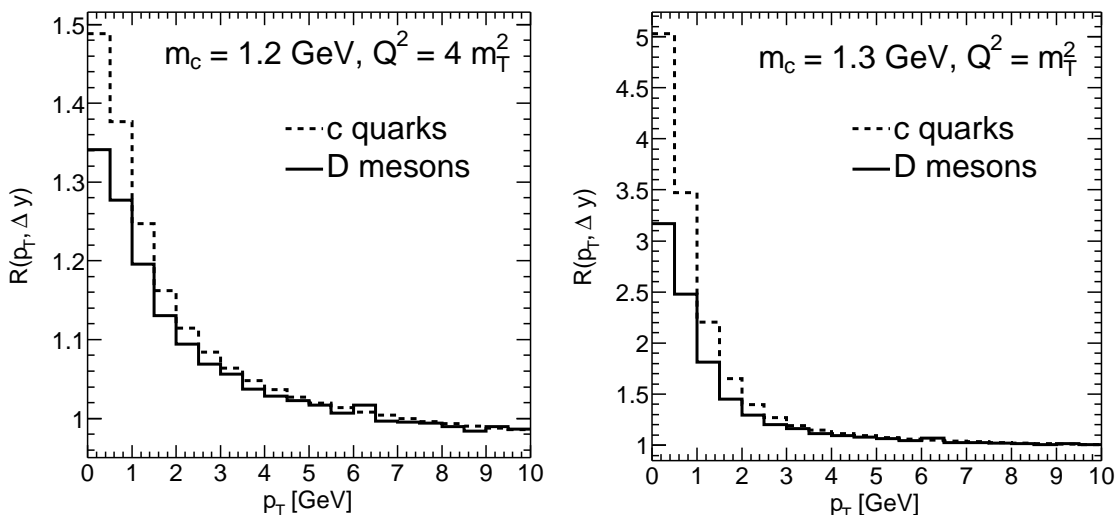


Figure 1: Enhancement factor $R(p_T, \Delta y)$ for charm quarks (dashed histogram) and for D ($\equiv D^+, D^0$) mesons (solid histogram), obtained after PYTHIA string fragmentation. The left-hand side shows the result for $m_c = 1.2$ GeV and $Q^2 = 4m_T^2$ while the right-hand side is the result for $m_c = 1.3$ GeV and $Q^2 = m_T^2$.

$p_T \gtrsim p_T^D$, where the charm enhancement is smaller. The D enhancement also vanishes with increasing transverse momenta, like the charm enhancement.

4 D^0 reconstruction in pp collisions with ALICE

The transverse momentum distribution of D^0 mesons produced at central rapidity, $|y| < 1$, can be directly measured from the exclusive reconstruction of $D^0 \rightarrow K^-\pi^+$ decays (and charge conjugates) in the Inner Tracking System (ITS), Time Projection Chamber (TPC) and Time Of Flight (TOF) detectors of the ALICE barrel, $|\eta| < 0.9$ [13]. The main feature of the D^0 decay topology is the presence of two tracks displaced from the interaction point by, on average, $50 \mu\text{m}$, for $p_T^D \simeq 0.5$ GeV, to $120 \mu\text{m}$, for $p_T^D \gtrsim 5$ GeV. Such displacement can be resolved with the ALICE tracking detectors and thus a large fraction of the combinatorial background in the $K^\mp\pi^\pm$ invariant mass distribution can be rejected. The low value of the magnetic field, 0.4 T, and the K/π separation in the TOF detector extend the D^0 measurement down to $p_T^D \sim 0$. The analysis strategy and the pertinent selection cuts were studied with a realistic, detailed simulation of the detector geometry and response, including the main background sources [15, 22].

The expected ALICE performance for pp collisions at $\sqrt{s} = 14$ TeV is summarized in Fig. 2 where the estimated relative uncertainties are reported as a function of p_T^D . The main contributions to the p_T -dependent systematic error (triangles) are the detector acceptance and reconstruction efficiency corrections (squares), $\simeq 10\%$, and the correction for feed-down from bottom decays, $B \rightarrow D^0 + X$ (open circles), $\simeq 8\%$. The

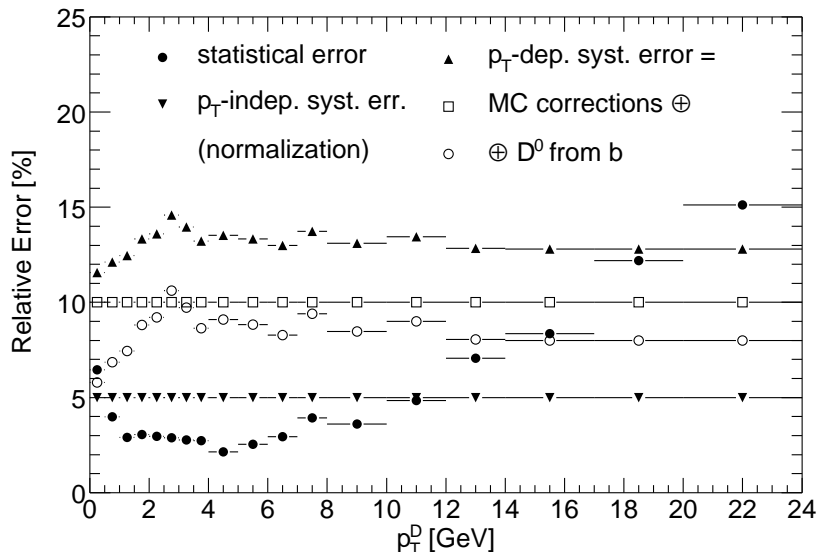


Figure 2: Estimated relative uncertainties on the measurement of the D^0 differential cross section in pp collisions at the LHC with ALICE [15]. Statistical uncertainties correspond to 10^9 minimum-bias pp events (an ≈ 9 month run with a luminosity of $\approx 5 \times 10^{30} \text{ cm}^{-2}\text{s}^{-1}$).

latter is estimated based on the present 70–80% theoretical uncertainty in the $b\bar{b}$ cross section at LHC energies [23]. However, we expect this uncertainty to be significantly reduced by the measurement of B decays to single electrons, $B \rightarrow e^\pm + X$, in ALICE [23]. The p_T -independent systematic error introduced by normalization to the pp inelastic cross section (inverted triangles) is also reported. This cross section will be measured by the TOTEM experiment [24] with an $\simeq 5\%$ uncertainty.

The statistical error corresponding to 10^9 minimum-bias pp events (filled circles), an ≈ 9 month run with a luminosity of $\approx 5 \times 10^{30} \text{ cm}^{-2}\text{s}^{-1}$, is smaller than or on the order of the p_T -dependent systematic error up to $p_T^D \simeq 24 \text{ GeV}$ for the alternative NLO cross section calculated using $m_c = 1.2 \text{ GeV}$, $Q^2 = 4m_T^2$ and the CTEQ6 PDFs with no enhancement. The relative statistical error depends on the charm cross section, as we now explain. For a given D^0 p_T^D or p_T^D range, the statistical error is the error on the number of real D^0 (\bar{D}^0) mesons in the $K^\mp\pi^\pm$ invariant mass distribution, the signal, $S(p_T^D)$. The error is equal to $\sqrt{S(p_T^D) + B(p_T^D)}/S(p_T^D)$ where $B(p_T^D)$ is the number of background candidates in the D^0 mass region. Then, at low p_T^D , the error is $\approx \sqrt{B(p_T^D)}/S(p_T^D) \propto 1/(d\sigma_D/dp_T^D)$ since the invariant mass distribution is dominated by combinatorial background. At high p_T^D , the background is negligible and the error becomes $\approx 1/\sqrt{S(p_T^D)} \propto 1/\sqrt{d\sigma_D/dp_T^D}$. In our subsequent results, the statistical errors are calculated taking this cross section dependence into account.

5 Sensitivity to the enhancement

Figure 3 shows the double-differential D^0 cross section, $d^2\sigma_D/dp_T^D dy$, in $|y| < 1$ as a function of the transverse momentum. The points represent the expected “data” measured by ALICE, obtained from the alternative NLO cross section scaled by the enhancement factor $R(p_T, \Delta y)$ defined in Eq. (7), and modified by string fragmentation. The solid and dashed curves are obtained by applying string fragmentation to the alternative NLO and standard NLO $c\bar{c}$ cross sections, respectively. Thus, the “data” points include the enhancement while the curves do not. The horizontal error bars indicate the bin width, the vertical error bars represent the statistical error and the shaded band gives the p_T -dependent systematic error. The 5% p_T -independent systematic error on the normalization is not shown. The left-hand side shows the results for $m_c = 1.2$ GeV and $Q^2 = 4m_T^2$ while the right-hand side shows those for $m_c = 1.3$ GeV and $Q^2 = m_T^2$. The standard NLO cross section, Eq. (5), and the $\mathcal{O}(\alpha_s^3)$ contribution to the alternative NLO cross section, Eq. (4), were calculated using the HVQMNR code [25] with CTEQ6M and $\Lambda_{\text{QCD}}^{(4)} = 0.326$ GeV. The LO contribution to the alternative NLO cross section, Eq. (2), was calculated using the CTEQ61L PDFs. Fragmentation was included as described in Section 3. The enhancement, the difference between the data and the solid curve visible for $p_T^D \lesssim 3$ GeV, is more pronounced for the larger mass and lower scale, shown on the right-hand side of Fig. 3.

There is a significant difference between the alternative and standard NLO distributions. Part of the difference is due to the one- and two-loop evaluations of α_s since $\alpha_s^{2\text{L}} < \alpha_s^{1\text{L}}$. This decrease will in turn reduce the $\mathcal{O}(\alpha_s^3)$ contribution to the alternative NLO result relative to the LO component of Eq. (2). In addition, the standard NLO cross section would be reduced overall relative to a calculation with the same $\Lambda_{\text{QCD}}^{(4)}$ at LO and NLO. However, these factors alone cannot explain the rather large difference between the standard and alternative NLO cross sections at low p_T^D . The most important contribution is the large differences between the LO and NLO gluon distributions, especially at low scales. The slope of the CTEQ61L gluon distribution at $Q^2 = 1.69$ GeV² with x is very small until $x > 0.01$. On the other hand, the CTEQ6M gluon x slope is large and has the opposite sign relative to CTEQ61L for $x < 0.04$. The ratio of the two sets at $x \approx 10^{-5}$ is very large, CTEQ61L/CTEQ6M ≈ 100 . At $Q^2 = 5.76$ GeV², the scale corresponding to $4m_c^2$ with $m_c = 1.2$ GeV, this ratio decreases to a factor of two. We note that at fixed-target energies, $\sqrt{s} \leq 40$ GeV, the standard and alternative NLO results are indistinguishable from each other since the LO and NLO gluon distributions are rather similar in this relatively high x region, $0.05 \leq x \leq 0.1$.

In order to address the question of the experimental sensitivity to the effect of nonlinear gluon evolution on low- p_T charm production, we consider, as a function of p_T^D , the ratio of the simulated data, including the enhancement, to alternative NLO calculations using a range of m_c and Q^2 along with PYTHIA string fragmentation. We denote this ratio as “Data/Theory”. Thus, given the measured D^0 p_T distribution, we try to reproduce this result with NLO calculations employing recent linearly-evolved

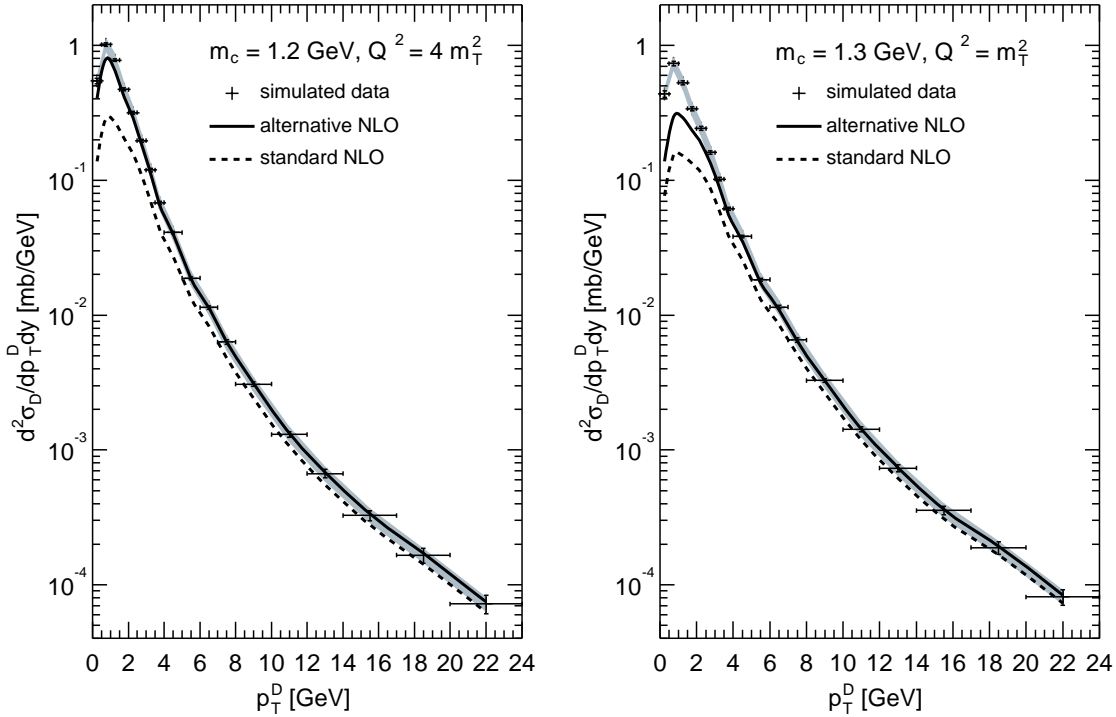


Figure 3: Comparison of the simulated ALICE data generated from $R(p_T, \Delta y)d\sigma_{\text{NLO}}^{\text{alt}}$ with the alternative (solid) and standard (dashed) NLO calculations. The effect of string fragmentation is included in the “data” points as well as in the curves. The left-hand side shows the result for $m_c = 1.2$ GeV and $Q^2 = 4m_T^2$ while the right-hand side is the result for $m_c = 1.3$ GeV and $Q^2 = m_T^2$. The error bars on the data represent the statistical error and the shaded band represents the p_T -dependent systematic error. The 5% normalization error is not shown.

PDFs and tuning m_c and Q^2 . We note that these parameters are not really free but are bounded by the range $1.2 \lesssim m_c \lesssim 1.8$ GeV and $1 \lesssim Q^2/m_T^2 \lesssim 4$, as described in Section 2 and in Ref. [10].

Since the enhancement has disappeared for $p_T^D \gtrsim 5$ GeV, we refer to this unenhanced region as high p_T^D . The p_T^D region below 5 GeV, where the enhancement is important, is referred to as low p_T^D . If no set of parameters can describe both the high- and low- p_T^D components of the distribution equally well, and, if the set that best reproduces the high- p_T^D part underestimates the low- p_T^D part, this would be a strong indication of the presence of nonlinear effects.

The Data/Theory plots are shown in Fig. 4. The points with the statistical (vertical bars) and p_T -dependent systematic (shaded region) error correspond to the data of Fig. 3, including the enhancement, divided by themselves, depicting the sensitivity to the theory calculations. The black squares on the right-hand sides of the lines Data/Theory = 1 represent the 5% p_T -independent error on the ratio coming from the cross section normalization. As clearly shown in Fig. 2, this error is, however, negligible with respect to the present estimates of the other systematic uncertainties ($\simeq 13\%$).

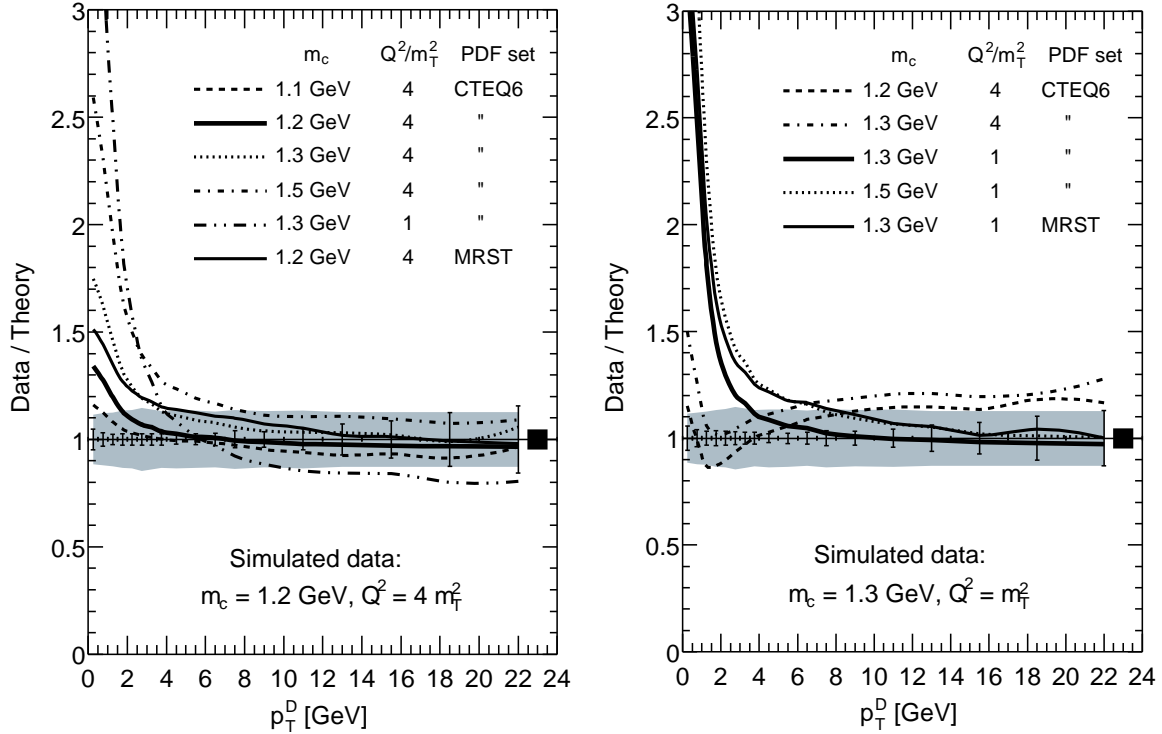


Figure 4: Ratio of the generated ALICE data relative to calculations of the alternative NLO cross sections with several sets of parameters and PYTHIA string fragmentation. The left-hand side shows the result for $m_c = 1.2 \text{ GeV}$ and $Q^2 = 4m_T^2$ while the right-hand side is the result for $m_c = 1.3 \text{ GeV}$ and $Q^2 = m_T^2$.

On the left-hand side, the thick solid curve with $m_c = 1.2 \text{ GeV}$ and $Q^2 = 4m_T^2$ best agrees with the high- p_T^D ratio by construction since $R \approx 1$ at large p_T^D . It also shows the effect of the enhancement well beyond the error band for $p_T^D \lesssim 2 \text{ GeV}$. Better agreement with the data over the entire p_T^D range can be achieved only by choosing a charm quark mass lower than 1.2 GeV , below the nominal range of charm masses, as illustrated by the dashed curve for $m_c = 1.1 \text{ GeV}$. Higher masses with $Q^2 = 4m_T^2$ produce much larger Data/Theory ratios than the input distribution. Choosing e.g. $m_c = 1.8 \text{ GeV}$ (not shown) would give a larger Data/Theory ratio than the $m_c = 1.5 \text{ GeV}$ result (dot-dashed curve). The ratio with $m_c = 1.3 \text{ GeV}$ and $Q^2 = m_T^2$ (dot-dot-dashed curve) gives a much larger ratio at low p_T^D and drops below the data for $p_T^D > 8 \text{ GeV}$.

We have checked how the results change when the renormalization and factorization scales are separated. When $m_c = 1.3 \text{ GeV}$, $Q_R^2 = m_T^2$ and $Q_F^2 = 4m_T^2$, the faster evolution of the higher Q_F^2 and the larger $\alpha_s(Q_R^2)$ resulting from the lower Q_R^2 leads to reasonable agreement between data and theory at low p_T^D . However, at high p_T^D , the theory distribution is harder so that the Data/Theory ratio drops below the error band for $p_T^D > 2 \text{ GeV}$. On the other hand, when $m_c = 1.3 \text{ GeV}$, $Q_R^2 = 4m_T^2$ and $Q_F^2 = m_T^2$, the theory cross section is reduced relative to the data and the Data/Theory ratio is

above the error band over all p_T^D .

We also present the ratio using the MRST parton densities (MRST2001 LO [4] in Eq. (2) and MRST2002 NLO [26] in Eq. (4)) with $m_c = 1.2$ GeV and $Q^2 = 4m_T^2$. We find that this result, the thin solid curve, also agrees reasonably well with the CTEQ6 results shown in the thick solid curve for the same m_c and Q^2 . Thus, the enhancement seems to be rather independent of the PDF. The CTEQ61L and the MRST2001 LO distributions are similar at low x , suggesting that PDFs based on this MRST set would produce an enhancement like that of Ref. [10]. However, the MRST2002 NLO and CTEQ6M NLO gluon distributions are very different at low x . The MRST2002 NLO gluon distribution is negative at low scales while the CTEQ6M gluon distribution goes to zero as $x \rightarrow 0$. Thus the effects of nonlinear evolution at NLO could be considerably different.

On the right-hand side of Fig. 4, with $m_c = 1.3$ GeV and $Q^2 = m_T^2$, the thick solid curve, employing the same parameters as the data, gives the best agreement at high p_T^D . We note that even though the results with $Q^2 = 4m_T^2$ and $m_c \leq 1.3$ GeV lie closer to the data at low p_T^D and within the combined statistical and systematic error at higher p_T^D , the curves with these parameters have the wrong slopes for $p_T^D \lesssim 8$ GeV. The systematic errors are more likely to shift the data points up or down as a whole rather than twist the p_T^D shape. The statistical sensitivity is expected to be good enough to distinguish the difference in curvature. Varying Q_F^2 and Q_R^2 separately results in similarly poor agreement as that noted for $m_c = 1.2$ GeV and $Q^2 = 4m_T^2$. Finally, the results obtained with the MRST PDFs, shown in the thin solid line, do not alter the conclusions already drawn for CTEQ6.

6 Conclusions

With constraints from HERA, the nonlinear DGLAP+GLRMQ evolution at LO leads to an enhancement of the free proton gluon distributions at $x \lesssim 0.01$ and $Q^2 \lesssim 10$ GeV² relative to DGLAP-evolved LO sets such as CTEQ61L. Consequently, charm hadroproduction at $\sqrt{s} \gtrsim 1$ TeV should be larger than expected from DGLAP-evolved PDFs alone [10]. In this paper, we have studied whether the EHKQS gluon distributions [7] could generate an observable D meson enhancement in pp collisions at the LHC. Since larger x values are probed at lower energy colliders, the enhancement described here would be reduced. At RHIC, $\sqrt{s} = 200$ GeV, the effect is too small to be reliably observed. However, D measurements at the Tevatron, $\sqrt{s} = 1.96$ TeV, may allow to detect an enhancement if the minimum p_T^D was lowered to ≈ 1 GeV.

In order to consider more realistic p_T^D distributions and yields, we have calculated the NLO contribution to charm production using the HVQMNR code [25]. Since the LO EHKQS PDFs cannot be used consistently with the NLO matrix elements, we assume the charm enhancement is the same at LO and NLO. We note that nonlinear effects on the NLO gluon distributions may be smaller than at LO, thus reducing the NLO charm enhancement. Therefore, our results may be considered upper limits of

the NLO D enhancement. Note also that if NLO DGLAP+GLR MQ PDFs that fit the small- x and small- Q^2 HERA data were available, it would be possible to base our analysis on the standard NLO charm cross section instead of the “alternative NLO” result defined in Eq. (6). Improved gluon distributions at low x and Q^2 may make the standard and alternative NLO results more similar at high energies, as they are at lower \sqrt{s} where x is larger.

Using the EHKQS LO PDFs and LO matrix elements for charm quark production and PYTHIA string fragmentation for D meson hadronization, we have demonstrated that more than half of the charm enhancement relative to calculations with the CTEQ61L LO PDFs indeed survives to the D mesons. In the most optimistic case, $m_c = 1.3$ GeV and $Q^2 = m_T^2$, the factor of five charm enhancement at $|y| \leq 1$ and $p_T \rightarrow 0$ is reduced to a factor of three at $p_T^D \rightarrow 0$. For larger values of m_c and Q^2 , the charm enhancement is smaller because the gluon enhancement due to nonlinear evolution decreases with increasing Q^2 .

The D meson enhancement, however, drops rapidly with transverse momentum so that for $p_T^D \sim 5$ GeV it is only a few percent. Therefore, D measurement capability at small p_T^D is necessary to verify the effect experimentally. The ALICE detector can do this through direct D^0 reconstruction in the $K^-\pi^+$ decay channel. We have demonstrated, using the error analysis of Ref. [15], that, in the most optimistic case, the enhancement can be detected above the experimental statistical and systematic errors. The sensitivity of the D enhancement to the scale has also been considered and we have shown that when the charm mass is somewhat smaller, $m_c = 1.2$ GeV, but the scale is larger, $Q^2 = 4m_T^2$, it is more difficult to detect the enhancement over the experimental uncertainties. The ALICE sensitivity to D meson production at very low transverse momentum may further improve by combining the $D^0 \rightarrow K^-\pi^+$ measurement with those of $D^+ \rightarrow K^-\pi^+\pi^+$ and $D^0 \rightarrow K^-\pi^+\rho^0$. A fast-simulation feasibility study of $D^+ \rightarrow K^-\pi^+\pi^+$ reconstruction [27] indicates that a performance similar to that of $D^0 \rightarrow K^-\pi^+$ could be achieved. More detailed analyses, currently in progress, will assess the low- p_T^D reach of this channel.

Acknowledgments: The work of A.D. and M.B. was carried out within the ALICE Collaboration, of which they are members, and using the software framework developed by the off-line project. A.D. and M.B. acknowledge the ALICE off-line group and the Physics Coordinator K. Šafařík for support and useful discussions. The work of R.V. was supported in part by the Director, Office of Energy Research, Division of Nuclear Physics of the Office of High Energy and Nuclear Physics of the U. S. Department of Energy under Contract Number DE-AC03-76SF00098. K.J.E. and V.J.K. gratefully acknowledge the financial support from the Academy of Finland, projects 50338, 80385 and 206024.

References

- [1] Y. L. Dokshitzer, Sov. Phys. JETP **46** (1977) 641 [Zh. Eksp. Teor. Fiz. **73** (1977) 1216]; V. N. Gribov and L. N. Lipatov, Yad. Fiz. **15** (1972) 781 [Sov. J. Nucl. Phys. **15** (1972) 438]; V. N. Gribov and L. N. Lipatov, Yad. Fiz. **15** (1972) 1218 [Sov. J. Nucl. Phys. **15** (1972) 675]; G. Altarelli and G. Parisi, Nucl. Phys. B **126** (1977) 298.
- [2] C. Adloff *et al.* [H1 Collaboration], Eur. Phys. J. C **21** (2001) 33 [arXiv:hep-ex/0012053].
- [3] A. D. Martin, R. G. Roberts, W. J. Stirling and R. S. Thorne, arXiv:hep-ph/0308087.
- [4] A. D. Martin, R. G. Roberts, W. J. Stirling and R. S. Thorne, Eur. Phys. J. C **23** (2002) 73 [arXiv:hep-ph/0110215].
- [5] L. V. Gribov, E. M. Levin and M. G. Ryskin, Nucl. Phys. B **188** (1981) 555; L. V. Gribov, E. M. Levin and M. G. Ryskin, Phys. Rept. **100** (1983) 1; A. H. Mueller and J. w. Qiu, Nucl. Phys. B **268** (1986) 427.
- [6] K. J. Eskola, H. Honkanen, V. J. Kolhinen, J. w. Qiu and C. A. Salgado, arXiv:hep-ph/0302185, in A. Accardi *et al.*, “Hard probes in heavy ion collisions at the LHC: PDFs, shadowing and pA collisions,” ed. K.J. Eskola, arXiv:hep-ph/0308248.
- [7] K. J. Eskola, H. Honkanen, V. J. Kolhinen, J. w. Qiu and C. A. Salgado, Nucl. Phys. B **660** (2003) 211 [arXiv:hep-ph/0211239].
- [8] J. Pumplin, D. R. Stump, J. Huston, H. L. Lai, P. Nadolsky and W. K. Tung, JHEP **0207** (2002) 012 [arXiv:hep-ph/0201195].
- [9] D. Stump, J. Huston, J. Pumplin, W. K. Tung, H. L. Lai, S. Kuhlmann and J. F. Owens, arXiv:hep-ph/0303013.
- [10] K. J. Eskola, V. J. Kolhinen and R. Vogt, Phys. Lett. B **582** (2004) 157 [arXiv:hep-ph/0310111].
- [11] R. Vogt [Hard Probe Collaboration], Int. J. Mod. Phys. E **12** (2003) 211 [arXiv:hep-ph/0111271].
- [12] R. Vogt, in proceedings of the 18th Winter Workshop on Nuclear Dynamics, edited by R. Bellwied *et al.*, Nassau, The Bahamas, 2002, p. 253.
- [13] ALICE Detector, Technical Proposal, CERN/LHCC 95-71.
- [14] T. Sjöstrand, P. Edén, C. Friberg, L. Lönnblad, G. Miu, S. Mrenna and E. Norrbin, Comput. Phys. Commun. **135** (2001) 238 [arXiv:hep-ph/0010017].

- [15] A. Dainese, Ph.D. Thesis, arXiv:nucl-ex/0311004.
- [16] B. L. Combridge, Nucl. Phys. B **151** (1979) 429; R.K. Ellis, in *Physics at the 100 GeV Scale*, Proc. of the 17th SLAC Summer Institute, Stanford, California, 1989, edited by E.C. Brennan (SLAC Report No. 361) 45.
- [17] H. L. Lai *et al.* [CTEQ Collaboration], Eur. Phys. J. C **12** (2000) 375 [arXiv:hep-ph/9903282].
- [18] R. Vogt, Heavy Ion Phys. **17** (2003) 75 [arXiv:hep-ph/0207359].
- [19] N. Kidonakis, E. Laenen, S. Moch and R. Vogt, Phys. Rev. D **67** (2003) 074037.
- [20] A. D. Martin, R. G. Roberts, W. J. Stirling and R. S. Thorne, Eur. Phys. J. C **4** (1998) 463 [arXiv:hep-ph/9803445]; A. D. Martin, R. G. Roberts, W. J. Stirling and R. S. Thorne, Phys. Lett. B **443** (1998) 301 [arXiv:hep-ph/9808371].
- [21] C. Peterson, D. Schlatter, I. Schmitt and P. Zerwas, Phys. Rev. D **27** (1983) 105.
- [22] N. Carrer, A. Dainese and R. Turrisi, J. Phys. G **29** (2003) 575.
- [23] M. Bedjidian *et al.*, “Hard Probes in Heavy Ion Collisions at the LHC: Heavy Flavor Physics”, eds. R. Vogt and S. Frixione, arXiv:hep-ph/0311048.
- [24] TOTEM, Total cross section, elastic scattering and diffractive dissociation at the LHC: Technical Proposal, CERN-LHCC-99-007; LHCC-P-5 (1999).
- [25] M. Mangano, P. Nason and G. Ridolfi, Nucl. Phys. B **373** (1992) 295.
- [26] A. D. Martin, R. G. Roberts, W. J. Stirling and R. S. Thorne, Phys. Lett. B **531** (2002) 216 [arXiv:hep-ph/0201127].
- [27] ALICE Inner Tracking System, Technical Design Report, CERN/LHCC 99-12.